5th INTERNATIONAL CONFERENCE ON

Optical Characterization of Materials

MARCH 17th – 18th, 2021
KARLSRUHE | GERMANY

J. BEYERER | T. LÄNGLE (Eds.)

KIT Scientific Publishing

Jürgen Beyerer | Thomas Längle (Eds.)

OCM 2021

5th International Conference on Optical Characterization of Materials

March 17th – 18th, 2021
Karlsruhe | Germany

OCM 2021

5th International Conference on Optical Characterization of Materials

March 17th – 18th, 2021
Karlsruhe | Germany

Edited by
Jürgen Beyerer | Thomas Längle

KIT Scientific Publishing

Veranstalter

Fraunhofer Institut of Optronics,
System Technologies and Image Exploitation IOSB
c/o Karlsruhe Center for Material Signatures KCM
Fraunhoferstraße 1, 76131 Karlsruhe

Dieser Tagungsband ist auch als Onlineversion abrufbar unter
http://dx.doi.org/10.5445/KSP/1000128686

Impressum

Scientific Publishing

Karlsruher Institut für Technologie (KIT)
KIT Scientific Publishing
Straße am Forum 2
D-76131 Karlsruhe

www.ksp.kit.edu

Print on Demand 2021 – Gedruckt auf FSC-zertifiziertem Papier

ISSN 2510-7240
ISBN 978-3-7315-1081-9
DOI 10.5445/KSP/1000128686

Fine metal-rich waste stream characterization based on RGB data: Comparison between feature-based and deep learning classification methods

Nils Kroell, Kay Johnen, Xiaozheng Chen, and Alexander Feil

Department of Anthropogenic Material Cycles, RWTH Aachen University, Wüllnerstraße 2, 52062 Aachen

Abstract *Background:* Material compositions in the recycling industry are currently determined by manual sorting, which is time intensive and shows subjective influences. For an automated, sensor-based material flow characterization a particle-based material classification is necessary. *Aim:* The classification of metal-containing fine-fractions based on RGB images with different machine learning (ML) techniques is investigated on two created datasets A (12,480 images) and B (19,498 images). *Method:* Two approaches are compared: In approach I, images are firstly pixel- and then object-based classified with six different ML models on three color spaces. In approach II, images are classified by six different convolutional neural networks (CNNs). *Results:* The classification of dataset A was possible with high accuracy ($>$ 99.8 %) for both approaches and chosen ML algorithms were of minor importance. For dataset B, approach I achieved an accuracy of 78.2 % $\pm$ 2.0 %, and chosen ML algorithms were of higher importance for object-based classification. In approach II, the best-performing CNN achieved an accuracy of 80.4 % $\pm$ 4.2 % and a top-3 score of 94.2 % $\pm$ 2.6 %. *Conclusion:* Results from existing studies for coarser particle sizes can be transferred to fine fractions. Further research is needed to improve the classification of dataset B, e. g. by adding instances to less frequent classes and applying deeper CNNs.

Keywords Sensor-based material flow characterization, fine fractions, recycling, metals, RGB, classification, machine learning, deep learning, convolutional neural networks.

1 Introduction

In the European Union, around 15.7 million Mg of non-ferrous (NF) metal-containing waste was generated in 2016 [1]. Recycling of valuable materials inside substitutes primary resources and therefore, achieves environmental benefits [2]. For example, recycling of aluminium saves 95 % of the used energy and reduces greenhouse gas emissions by 92 % compared to primary production [3].

Currently, about one-third of all NF metals produced originate from secondary raw material sources [4]. With rising climate change [5], decreasing valuable material contents of primary resources [6, p. 47] and an increasing demand for raw materials from emerging and developing countries [7], a transition towards a circular economy and thus an increased exploitation of secondary raw materials is necessary [8].

During the processing of metal scrap, metal-containing fine fractions ($\leq$ 20 mm) are generated as a by-product [9, p. 263f], which can contain up to 30 wt% metals [10] but are insufficiently recovered to date [10]. For an optimal recovery of the contained metals as well as a quality assurance of generated product streams, the material composition needs to be known. Currently, samples are analysed by manual sorting [11, p. 51], which is time and cost intensive and often shows subjective influences from the manual sorter [12]. As a result, material flows are often characterized on an irregular basis and sample amounts are statistically limited.

A sensor-based material characterization (SBMC) offers the possibility to overcome these limitations, as it minimizes subjective influences, and material flows can be monitored in nearly real-time. The first step of such an SBMC is the classification of individual particles to given material classes. In a second step, the predicted material classes can be combined with individual particle masses in order to derive mass-based material compositions for e. g. process control or automated quality assurance.

NF metals can be classified by different sensors, e. g. X-ray transmission or fluorescence, laser induced breakdown spectroscopy, induction (IND) or color sensors (RGB as well as hyperspectral imaging (HSI)) [13]. In comparison to other available sensors, RGB sensors are available in high resolution, technically matured and often by one order of magnitude or more cost-effective and thus focus of this study.

2 Related Work

While sensor-based sorting of metals is state of the art [13], the SBMC of metal-containing waste streams is an active area of research. For coarse particle sizes ($>$ 20 mm), the classification based on RGB images has been researched in several studies:

- Wang et al. (2019) [14] demonstrated the classification of aluminium and copper from shredded end-of-life vehicles based on particle related features. With a support vector machine (SVM), an object-based classification score of 96.64 % was achieved.
- Dang et al. (2019) [15] compared the classification of metal objects with convolutional neural networks (CNNs). With an AlexNet-architecture [16], the material classes copper, brass and other metals could be classified with an object-based accuracy of 97.15 %.
- Karbasi et al. (2018) [17] studied the classification of particles from shredded waste of electrical and electronic equipment (WEEE) using a ResNet-architecture [18]. For the three material classes printed circuit boards (PCB), plastics and cables, an object-based accuracy of 98 % was achieved.

Studies on the classification of metal-containing fine fractions ($\leq$ 20 mm) until now have focused on the application of hyperspectral imaging or a combination of multiple sensors, see Table 8.1. The classification of these fine fractions only based on RGB images has not been investigated yet, which is the research gap addressed here.

Table 8.1: Existing studies on optical classification of metal-containing fine fractions; 3DLT: 3D laser triangulation, * sorting rate, ** product purity.

Study	Date	Material origin	Sensor	Classification accuracy: pixel-based	object-based	
Candiani et al.	2017	PCB	HSI	87.7 %	97.2 %	[19]
Barnabé et al.	2015	WEEE	HSI	83.9 %	96.0 %	[20]
Huang et al.	2010	NF metals	RGB + 3DLT	-	98.0 %*	[21]
Picon et al.	2009	WEEE	HSI	71.7 %	98.4 %	[22]
Kutila et al.	2006	NF metals	RGB + IND	-	80.0 %**	[23]

3 Material and Methods

Two machine learning (ML) approaches (I: ”feature-based classification” and II: ”deep learning”) are compared. For training and evaluation of the models, two datasets A and B were created.

3.1 Data Acquisition

Particle images were taken with a custom made test rig on a white paper background by a high-resolution RGB-camera (IDS U3-3800CP-C-HQ Rev.2) with a color depth of 12-bit and a resulting spatial resolution of 0.11 mm/Pixel. The recording area of 100 mm $\times$ 100 mm was illuminated from top by white LED-stripes (Samsung 2835 120 LED 12V IP20 4000K). For each particle, a front and back image was recorded.

3.2 Samples and Datasets

Dataset A contains standard components made of copper (Cu), grey metals (GM), brass (Msg) and black plastics (KS). Characteristic particle shapes and sizes are generated by comminuting the particles in a hammer mill and sieving them into the investigated particle size range of 3.15 mm to 10 mm ($\Delta t_{\text{sieving}} = 90$ s). In total, there are n = 12,480 images in the dataset (n_{Cu} = 4,016; n_{GM} = 2,120; n_{Msg} = 3,056; n_{KS} = 3,288), see Figure 3.1. After acquisition, the dataset was split in a train and test dataset with a train-test-split-ratio of 80 % : 20 %.

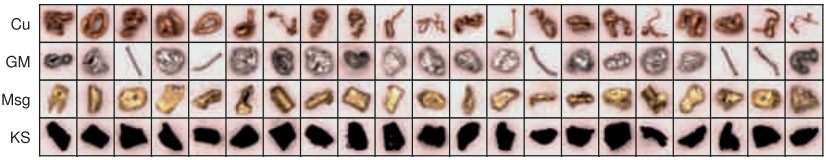

Figure 3.1: Exemplary images (cropped) for the four material classes of dataset A.

For dataset B, samples in the particle range 3 mm to 9 mm were collected from a metal-recovery plant in Germany according to LAGA PN 98 [24]. The samples were manually sorted in 22 material classes with a two stage process (see [12] for details). The final dataset contains

19,498 images, see Table 8.2 and Figure 3.2, and was split in a train and test dataset with a train-test-split-ratio of 75 % : 25 % to guarantee enough instances for less frequent classes in the test set.

Table 8.2: Number of images *n* in dataset B. +: Composite of the mentioned materials.

Material class	Abbreviation	*n*	Material class	Abbreviation	*n*
Copper	Cu	3,123	GM wires	GMKaAd_oS	38
Grey metals	GM	2,169	GM wires + plug	GMKaAd_mS	2
Brass	Msg	2,080	PCB	PCBA	864
Plastics	KS	2,453	GM + NM	GM_NM	195
Glass	Glas	48	Cu + NM	Cu_NM	893
Minerals	KSP	50	Msg + NM	Msg_NM	63
Residual	Rest	390	GM + Cu	GM_Cu	1,702
Cu wires	CuAd_oS	898	GM + Msg	GM_Msg	134
Cu wires + plug	CuAd_mS	174	Cu + Msg	Cu_Msg	291
Cu cables	CuKa_oS	30	GM + Cu + Msg	GM_Cu_Msg	62
Cu cables + plug	CuKa_mS	5	Complex	Komplex	54
				$\sum$	19,498

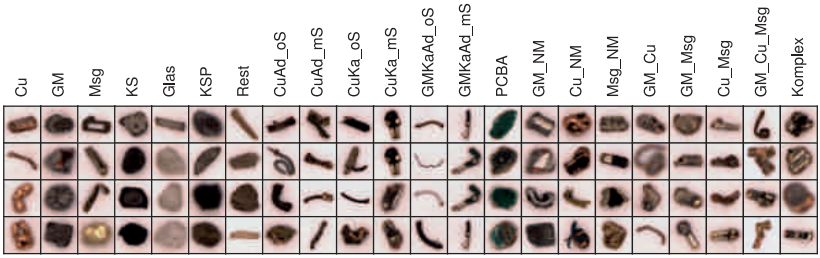

Figure 3.2: Exemplary images (cropped) for the 22 material classes of dataset B.

3.3 Preprocessing

The captured images were then preprocessed to improve the color representation. Preprocessing algorithms were implemented in *Python 3.7* in a *scikit-image* v0.17.1 [25] framework. Firstly, a Gaussian blur filter

with a standard deviation of $\sigma = 0.35$ was applied to reduce small artefacts from demosaicing during image acquisition. Secondly, a white balance based on a white reference image was applied to guarantee a neutral color representation. Thirdly, an spatial illumination correction based on the reference image ensured an uniform illumination.

To extract individual pixels for color classification, each captured image was segmented into background, shadows and particle trough thresholding the gray scale image and improving the segmentation result by a combination of morphological operations. For the color classification, 1,000 pixels per particle as well as 1,000 background pixels (850 pixels of white background and 150 shadows pixels) were randomly selected from each segmented image.

For the image classification with CNNs, quadratic image sections of the particle were extracted (cf. Figure 3.1 and 3.2). A minimum padding of 25 % of the respective particle bounding box size was ensured between particle and the border of the image section. All extracted image sections were rescaled to a size of 64 Pixel $\times$64 Pixel.

3.4 Approach I: Feature-Based Classification

The color classification was tested for three color spaces (RGB, HSV and L*a*b*). For dataset A, each color class represents a material class. For dataset B, the color classes BG, Cu, GM, Msg, KS, Glas, KS and Rest ('pure fractions') were defined, as the color of composite material classes (e. g. Cu + Msg) overlapped strongly with the pure fractions. Besides, characteristic colors of PCBA and KaAD (cables and wires) were extracted with a tomek link technique [26, p. 57]. All color classifiers were trained on 4,000 pixels per material class and 8,000 background pixels to avoid overfitting.

For object-based classification, shares of each classified color class as well as 50 dimensionless shape factors were considered, which were generated by normalizing shape measurements by the particle area A or its square root ($\sqrt{A}$). Shape measurements were extracted from the false-color image by a self-developed Python module named *eidos*[1].

For both pixel- and object-based classification, six ML classification algorithms, implemented in *scikit-learn* [27], were compared: k nearest

[1] `https://github.com/nilskroell/eidos`

neighbor (kNN), decision trees (DT), random forests (RF), AdaBoost (AB), SVM, neural networks (NN). For each model and classification task, a systematic grid search with a k-fold-cross-validation ($k = 5$) on the training dataset was conducted to find the optimal hyperparameter settings. All hyperoptimized models were evaluated on the test dataset.

3.5 Approach II: Deep Learning

For image classification, six different CNN architectures (Figure 3.3) were compared, implemented in *Keras* [28]. All hidden layers were equipped with a ReLU activation function and the final network output was normalized by a softmax function. During training, an Adam [29] optimizer with a learning rate of $\eta = 10^{-3}$ was used. Dataset A and B were trained for 15 and 20 epochs respectively with a mini batch size of 256 instances per iteration. L2-norm regularization ($\lambda = 10^{-3}$) as well as dropout layers with an dropout rate of 0.5 were applied to avoid overfitting, and the classification performance was evaluated by a categorical cross entropy cost function. To reduce the imbalance, downsampling was applied to material classes with more than 2,000 instances. All trained CNNs were evaluated on the test dataset.

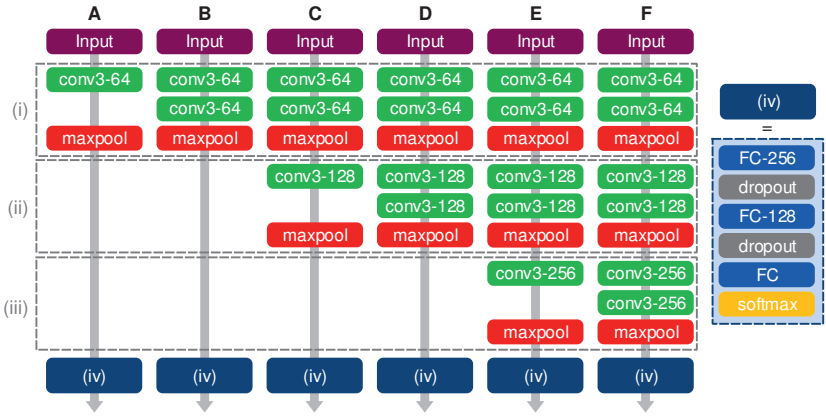

Figure 3.3: Investigated CNN architectures A-F consisting of input (64×64), fully connected (FC-$\langle n \rangle$), 3×3 convolutional (conv3-$\langle n \rangle$), 2×2 max pooling, dropout (0.5) and softmax activation layers; n: number of neurons/feature maps.

4 Results and Discussion

4.1 Approach I: Feature-Based Classification

The color classification of dataset A was possible with similar accuracies of $\geq$ 79.8 % for all models and colorspaces, see Table 8.3. On average, the L*a*b* color space with 86.1 % and a SVM model with 87.0 % achieved the best classification results. Because of the superior color classification, an object-based classification with 100 % accuracy could be achieved, e. g. by a plain kNN model, for dataset A.

Table 8.3: Accuracy for color classification of dataset A after hyperparameter optimization; 95 % confidence interval for all accuracies: $\pm$ 0.08 % to $\pm$ 0.18 %.

	kNN	**DT**	**RF**	**AB**	**SVM**	**NN**	mean
RGB	85.4 %	79.8 %	85.2 %	84.1 %	87.3 %	87.3 %	84.9 %
HSV	82.7 %	82.9 %	86.7 %	85.5 %	87.2 %	84.4 %	84.9 %
L*a*b*	85.3 %	85.2 %	86.9 %	85.6 %	86.7 %	87.1 %	**86.1 %**
mean	84.5 %	82.6 %	86.3 %	85.1 %	**87.0 %**	86.3 %	85.3 %

Based on the results above, the L*a*b* color space was chosen for the color classification of dataset B (Table 8.4). Here, the classification was more challenging with achieved test scores between 47.2 % (DT) and 51.1 % (kNN, SVM). As for dataset A, the chosen classification algorithm was of minor importance. Significant differences were found in the prediction time: The fasted model (DT) was with 13 ms/MPixel 714 times faster than the slowest one (AB; 9,278 ms/MPixel). Overall, a NN model showed the best combination of prediction time and accuracy and was thus the basis for subsequent object-based classification.

Test scores of the object-based classification of dataset B, based on extracted false-color shares and ten shape factors with highest feature importance (determined by χ^2-test on training data) are shown in Table 8.5. Here, the chosen algorithm was of higher importance with achieved accuracies ranging from 66.5 % (kNN) and 78.2 % (RF).

A closer look on the best-performing model (RF) in Figure 4.1a shows that the predictions differ significantly between different material classes. As expected, material classes with a higher number of instances can be significantly better classified than less frequent classes.

Table 8.4: Test scores and prediction time (Δt_{pred}) for color classification of dataset B after hyperparameter optimization in L*a*b* color space; CI: confidence interval.

	kNN	DT	RF	AB	SVM	NN
Accuracy	51.1 %	47.2 %	50.8 %	48.3 %	**51.1** %	51.0 %
95 %-CI	± 2.9 %	± 0.6 %	± 1.8 %	± 3.1 %	± **0.6 %**	± 0.7 %
Δt_{pred} [ms/MPixel]	1,234	**13**	3,250	9,278	5,589	196
95 %-CI [ms/MPixel]	± 29	± **4**	± 290	± 83	± 24	± 5

Table 8.5: Test scores for object-based classification of dataset B; CI: confidence interval.

	kNN	DT	RF	AB	SVM	NN
Accuracy	66.5 %	67.4 %	**78.2 %**	77.2 %	72.9 %	72.6 %
95 %-CI	± 3.6 %	± 2.0 %	± **2.0 %**	± 1.9 %	± 1.8 %	± 3.4 %

On average, pure fractions with an accuracy of 62.5 % could be far better classified than composite fractions (16.7 %). Providing different numbers of shape factors to the model (Figure 4.1b) revealed that the shape factors contributed little to the classification performance, which is primarily achieved by the extracted false color components.

4.2 Approach II: Deep Learning

As for the feature-based approach, the classification of dataset A with CNNs was possible with high accuracy ($>$ 98.8 %), see Table 8.6. Even simple CNN architectures showed a high accuracy.

Table 8.6: Test scores of the CNN architectures A-F for dataset A; CI: confidence interval.

CNN	A	B	C	D	E	F
Accuracy	99.59 %	**99.82** %	99.65 %	99.76 %	99.65 %	98.88 %
95 %-CI	± 1.19 %	± **0.84** %	± 1.21 %	± 0.87 %	± 0.87 %	± 1.61 %

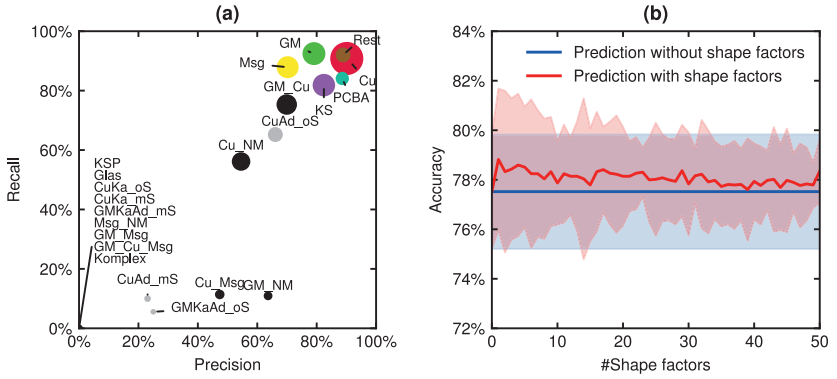

Figure 4.1: Object-based classification of the trained RF model on dataset B. **(a)** Accuracy by material class (circle area $\sim$ #instances), **(b)** influence of shape factors.

In contrast, training CNNs on dataset B turned out to be more challenging. For all six CNN architectures, the error rate did not converge after the initial planned 20 training epochs (see Figure 4.2), resulting in accuracies of $\leq$ 33.5 % when training all 22 material classes.

To optimize the classification result the architecture and training of CNN F was further adapted. Firstly, the number of neurons in the fully connected layer was increased to 1,024, which boosted the resulting accuracy to 48.9 % $\pm$ 3.6 %. Secondly, the number of training epochs was increased from 20 to 400. As shown in Figure 4.2a, the optimized CNN F* converged after about 200 training epochs and achieved an overall classification accuracy of 80.4 % $\pm$ 4.2 %. Furthermore, a strong correlation between the number of images in the training set and the classification performance (F1-score) per material class could be confirmed, see Figure 4.2b.

The activations in the six convolutional layers of CNN F* (Figure 4.4) show how CNN F* is able to abstract the particle characteristics with each layer. When considering the given probabilities for each prediction, CNN F* achieved a top-3 score of 94.2 % $\pm$ 2.6 %, i. e. for 94.2 % of the predictions the right material class was in the three material classes with the highest probability.

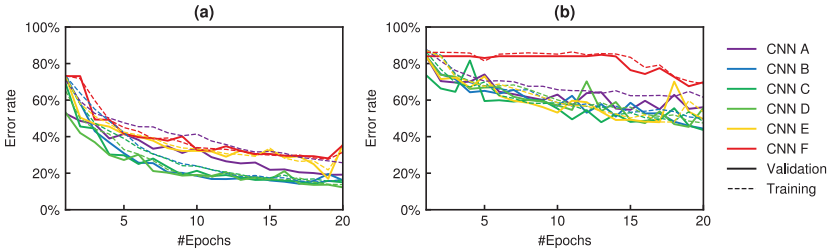

Figure 4.2: Training of CNN A-F for the classification of dataset B **(a)** with four selected material classes (Cu, GM, Msg, KS) and **(b)** all 22 material classes.

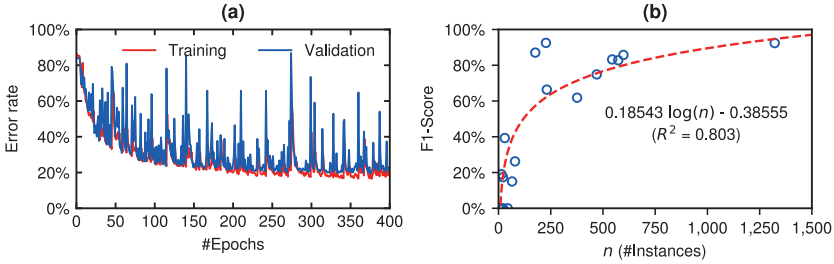

Figure 4.3: (a) Training of CNN F* with dataset B over 400 epochs, **(b)** correlation between number of instances per material class and F1-score for dataset B.

5 Conclusions and Outlook

In this research, the classification of two datasets A (12,480 images in four material classes) and B (19,498 images in 22 material classes) with a feature-based and deep learning approach was investigated. Our results show that a nearly perfect ($>$ 99.8 %) classification for all four material classes of dataset A could be achieved with both approaches, as particles of the different material classes can be clearly differentiated by their color in the RGB images. This indicates that classification results from coarse fraction can in general be transferred to fine fractions. The achieved classification results are better than existing studies on coarse fractions, most likely due to missing influences of different metal alloys or post-consumer waste characteristics, as comminuted standard components were used to create dataset A.

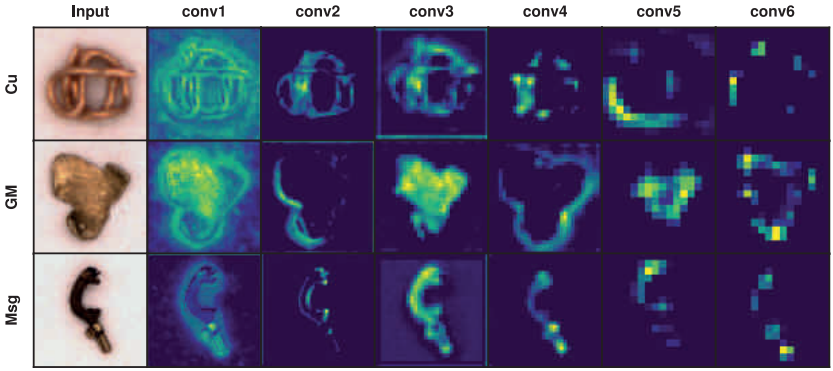

Figure 4.4: Selected convolutional feature maps of CNN F* when classifying dataset B.

In contrast, the classification of dataset B turned out to be quite challenging. Our best feature-based approach consisting of a pixel-based color classification with a neural network in the L*a*b* color space and a subsequent object-based classification with a random forest, achieved a classification accuracy of 78.2 % $\pm$ 2.0 %. A slightly better classification result was achieved by the deep learning approach with a 14 layer CNN with an accuracy of 80.4 % $\pm$ 4.2 % and an top-3 score of 94.2 % $\pm$ 2.6 %. To improve the classification of dataset B in the future we see potential for future research in the following points:

1. **Extension of dataset B:** For both classification approaches a strong correlation between the number of instances and the classification accuracy of material classes was found. Thus, extending dataset B with more images of less frequent material classes may improve the overall classification performance.

2. **Training of deeper CNNs:** Deeper CNN architectures may be advantageous in adapting to the complex particle characteristics of dataset B. Furthermore, existing CNN architectures or transfer learning may be applied to enhance the classification.

3. **Application of multi sensors:** While this study has focused on RGB images, new distinctive features for classification might be obtained by utilizing multiple sensors, e. g. RGB and induction or X-ray fluorescence/transmission.

References

1. Eurostat, "Abfallaufkommen nach Abfallkategorie, Gefährlichkeit und NACE Rev. 2 Tätigkeit." [Online]. Available: https://appsso.eurostat.ec.europa.eu/nui/show.do?dataset=env_wasgen&lang=de
2. B. K. Reck and T. E. Graedel, "Challenges in metal recycling," *Science (New York, N.Y.)*, vol. 337, no. 6095, pp. 690–695, 2012.
3. S. Grimes, J. Donaldson, and G. C. Gomez, "Report on the Environmental Benefits of Recycling." [Online]. Available: https://www.mgg-recycling.com/wp-content/uploads/2013/06/BIR_CO2_report.pdf
4. UNEP – International Resource Panel, "Report 2: Recycling Rates of Metals – A Status Report."
5. V. Masson-Delmotte, P. Zhai, H.-O. Pörtner, D. Roberts, J. Skea, and P. R. Shukla, "Global Warming of 1.5°C: An IPCC Special Report on the impacts of global warming of 1.5°C above pre-industrial levels and related global greenhouse gas emission pathways, in the context of strengthening the global response to the threat of climate change, sustainable development, and efforts to eradicate poverty."
6. M. Kranert, *Einführung in die Kreislaufwirtschaft*. Wiesbaden: Springer Fachmedien Wiesbaden, 2017.
7. A. Bloodworth and G. Gunn, "The future of the global minerals and metals sector : issues and challenges out to 2050," *Geosciences: BRGM's journal for a sustainable Earth*, vol. 15, pp. 90–97, 2012.
8. European Commission, "A new Circular Economy Action Plan for a cleaner and more competitive Europe." [Online]. Available: https://eur-lex.europa.eu/legal-content/EN/TXT/?uri=CELEX:52020DC0098
9. H. Martens, *Recyclingtechnik: Fachbuch für Lehre und Praxis*. Heidelberg: Spektrum Akademischer Verlag, 2011.
10. K. Johnen and A. Feil, "Untersuchung von Feinfraktionen aus metallhaltigen Abfallströmen," in *14. Recy & DepoTech-Konferenz : Montanuniversität Leoben, Österreich*.

11. “Technische Anleitung zur Verwertung, Behandlung und sonstigen Entsorgung von Siedlungsabfällen: TA Siedlungsabfall,” 14.05.1993.

12. K. Johnen, N. Kroell, and A. Feil, “Entwicklung einer Methodik zur Wertstoffgehaltsbestimmung von feinkörnigen Abfällen,” in *15. Recy & DepoTech-Konferenz : Montanuniversität Leoben, Österreich*.

13. A. Feil, T. Pretz, J. Julius, N. Go, M. Bosling, and K. Johnen, “Metal waste,” in *Waste*, T. M. Letcher and D. A. Vallero, Eds. Elsevier, 2019, pp. 211–223.

14. C. Wang, Z. Hu, Q. Pang, and L. Hua, “Research on the classification algorithm and operation parameters optimization of the system for separating non-ferrous metals from end-of-life vehicles based on machine vision,” *Waste management (New York, N.Y.)*, vol. 100, pp. 10–17, 2019.

15. T. L. Dang, T. Cao, and Y. Hoshino, “Classification of metal objects using deep neural networks in waste processing line,” *International Journal of Innovative Computing, Information and Control*, no. 15, pp. 1901–1912, 2019.

16. A. Krizhevsky, I. Sutskever, and G. E. Hinton, “ImageNet classification with deep convolutional neural networks,” *Communications of the ACM*, vol. 60, no. 6, pp. 84–90, 2017.

17. H. Karbasi, A. Sanderson, A. Sharifi, and C. Wilson, “Robotic Sorting of Shredded E-waste: Utilizing Deep Learning,” in *ICAI ′18*, H. R. Arabnia, D. d. La Fuente, E. B. Kozerenko, J. A. Olivas, and F. G. Tinetti, Eds. United States of America: CSREA Press, 2018, pp. 119–123.

18. K. He, X. Zhang, S. Ren, and J. Sun, “Deep Residual Learning for Image Recognition.” [Online]. Available: https://arxiv.org/pdf/1512.03385

19. G. Candiani, N. Picone, L. Pompilio, M. Pepe, and M. Colledani, “Characterization of Fine Metal Particles Derived from Shredded WEEE Using a Hyperspectral Image System: Preliminary Results,” *Sensors (Basel, Switzerland)*, vol. 17, no. 5, 2017.

20. P. Barnabé, G. Dislaire, S. Leroy, and E. Pirard, “Design and calibration of a two-camera (visible to near-infrared and short-wave infrared) hyperspectral acquisition system for the characterization of metallic alloys from the recycling industry,” *Journal of Electronic Imaging*, vol. 24, no. 6, p. 061115, 2015.

21. J. Huang, T. Pretz, and Z. Bian, “Intelligent solid waste processing using optical sensor based sorting technology,” in *2010 3rd International Congress on Image and Signal Processing*. IEEE, 2010, pp. 1657–1661.

22. A. Picon, O. Ghita, P. F. Whelan, and P. M. Iriondo, “Fuzzy Spectral and Spatial Feature Integration for Classification of Nonferrous Materials in

Hyperspectral Data," *IEEE Transactions on Industrial Informatics*, vol. 5, no. 4, pp. 483–494, 2009.

23. M. Kutila, J. Viitanen, and A. Vattulainen, *Scrap Metal Sorting with Colour Vision and Inductive Sensor Array: Proceedings 28-30 November 2005, Vienna, Austria*. Los Alamitos Calif.: IEEE Computer Society, 2006.
24. Länderarbeitsgemeinschaft Abfall, "LAGA PN 98: Richtlinie für das Vorgehen bei physikalischen, chemischen und biologischen Untersuchungen im Zusammenhang mit der Verwertung/Beseitigung von Abfällen," 2001.
25. S. van der Walt, J. L. Schönberger, J. Nunez-Iglesias, F. Boulogne, J. D. Warner, N. Yager, E. Gouillart, and T. Yu, "scikit-image: image processing in Python," *PeerJ*, vol. 2, p. e453, 2014.
26. M. Kubat, *An Introduction to Machine Learning*, 2nd ed. Cham: Springer International Publishing, 2017.
27. F. Pedregosa, G. Varoquaux, A. Gramfort, V. Michel, B. Thirion, O. Grisel, M. Blondel, P. Prettenhofer, R. Weiss, V. Dubourg, J. Vanderplas, A. Passos, D. Cournapeau, M. Brucher, M. Perrot, and E. Duchesnay, "Scikit-learn: Machine Learning in Python," *Journal of Machine Learning Research*, vol. 12, pp. 2825–2830, 2011.
28. F. Chollet, K. Allison, M. Wicke, S. Bileschi, P. Bailey, A. Gibson, J. J. Allaire, F. Rahman, F. Branchaud-Charron, T. Lee, and G. de Marmiesse, "Keras," 2015. [Online]. Available: https://keras.io
29. D. P. Kingma and J. Ba, "Adam: A Method for Stochastic Optimization." [Online]. Available: https://arxiv.org/pdf/1412.6980